Catalysis Communications 129 (2019) 105749

Contents lists available at ScienceDirect

Catalysis Communications

journal homepage: www.elsevier.com/locate/catcom

Short communication

Ag_2S-CoS hetero-nanowires terminated with stepped surfaces for improved oxygen evolution reaction

Changsoo Lee[a,1], Chulhee Lee[a,1], Kihyun Shin[b], Taeyoung Song[a], Hu Young Jeong[c], Duk Young Jeon[a,*], Hyuck Mo Lee[a,*]

[a] Department of Materials Science and Engineering, KAIST, 291 Daehak-ro, Yuseong-gu, Daejeon 34141, Republic of Korea
[b] Department of Chemistry, Institute for Computational Engineering and Sciences, University of Texas at Austin, Austin, TX 78712, United States
[c] UNIST Central Research Facilities (UCRF), UNIST, Ulsan 44919, Republic of Korea

ARTICLE INFO

Keywords:
Cobalt sulfide
Seeded growth
Stepped surface
Oxygen evolution reaction

ABSTRACT

Water electrolysis has received great attention for producing hydrogen, but sluggish kinetics of oxygen evolution reaction (OER) has remained a big challenge. Recently, cobalt sulfide materials have been widely explored as great choice in highly efficient electrocatalysts due to their good electrical conductivity and bi-functionality toward OER and hydrogen evolution reaction (HER). However, cobalt sulfide shows outstanding HER activity, but its OER activity should be improved. Herein, hexagonal-phase cobalt sulfide (CoS) nanowires with abundant stepped surfaces and defect sites were prepared via a seed-growth approach with silver sulfide (Ag_2S) nanoparticles. The Ag_2S-CoS hetero-nanowires (HNWs) exhibited excellent electrochemical performances for oxygen evolution reaction (overpotential = 275 mV, Tafel slope = 77.1 mVdec^{-1}, charge transfer resistance = 1.3 Ω) in 1.0 M KOH solution. The origin of superior activity was investigated using a combined experimental and theoretical approach. This work highlights the importance of surface defects for improving oxygen evolution reaction performance of water electrolysis.

1. Introduction

Hydrogen has received significant attention as a next-generation energy carrier [1] because it results in no CO_2 emission and has a higher energy-to-weight ratio (33.3 kWh kg^{-1}) [2] than other fossil fuels, such as coal, natural gas, and petroleum. Currently, most hydrogen is produced through a process called steam reforming using fossil fuels [3]. As an eco-friendly approach, water electrolysis has been studied intensively for a few decades. Water electrolysis can be divided into the hydrogen evolution reaction (HER, cathodic reaction) and the oxygen evolution reaction (OER, anodic reaction) [4,5]. The OER, which follows a 4-electron path, is significantly slower than the HER, which follows a 2-electron pathway [6]. Therefore, the OER determines the overall reaction rate of water electrolysis. Pt electrodes for the HER and precious metal oxides such as IrO_2 and RuO_2 for the OER have been considered state-of-the-art catalysts. Because of the high cost and poor stability of these catalysts, various alternatives must be developed.

Currently, transition metal chalcogenides, such as sulfide, phosphide and selenide, have received much attention as bifunctional electrocatalysts, showing activity for both the HER and the OER [7,8]. Among these materials, cobalt sulfide electrocatalysts have been studied intensively due to their superior electrical conductivity, acceptable price and excellent stability over a wide range of pH and voltage [9,10]. Cobalt sulfide shows outstanding HER activity [11], but its OER activity must be improved [12]. Cobalt sulfide has four kinds of crystalline structures: CoS, CoS_2, Co_3S_4, and Co_9S_8 [13]. The cobalt atoms are located in an octahedral site in CoS and CoS_2 and in both tetrahedral and octahedral sites in Co_3S_4 and Co_9S_8 [14]. Octahedral Co atoms are considered active sites in cobalt sulfide electrocatalysts for the OER. Ma et al. have reported the activity order of CoS_2 > Co_3S_4 > Co_9S_8 related to from the concentration of octahedral Co atoms [14]. Cai et al. have demonstrated the outstanding OER activity of disordered structures of CoS_2 nanocubes, which possess abundant exposed octahedral sites, and have shown the strong O-binding energy of defect sites of CoS_2 via density functional theory (DFT) calculations. Likewise, the cobalt sulfides have been widely exploited in many OER studies focusing on CoS_2, Co_3S_4 and Co_9S_8, but hexagonal phase CoS has been rarely studied excepting a few reports. The few reports investigated OER properties by combining Ni foam [15], MWCNT [9] and substituting phosphors [16]. Though they studied the hexagonal phase

* Corresponding authors.
E-mail addresses: dyj@kaist.ac.kr (D.Y. Jeon), hmlee@kaist.ac.kr (H.M. Lee).
[1] These authors contributed equally to this work.

https://doi.org/10.1016/j.catcom.2019.105749
Received 14 April 2019; Received in revised form 7 June 2019; Accepted 30 June 2019
Available online 02 July 2019

CoS, further studies on defect sites of the hexagonal phase CoS are still needed to develop high performance OER catalysts.

Nanowire structures have been adapted in many electrocatalytic applications, such as the OER, the HER, the oxygen reduction reaction (ORR), and CO_2 electroreduction [17,18]. The NW network has superior electrical conductivity, a high surface area, and better stability than nanoparticles (NPs). Li et al. have shown that jagged PtNi alloy nanowires exhibit 53-fold higher mass activity (13.6 A/mg_{pt}) for the ORR than 10 wt% Pt/C electrocatalysts [19]. Xu et al. have fabricated NiCoO nanowires for the OER and NiCoP nanowires for the HER, showing 248 mV and 101 mV overpotentials, respectively [20]. Therefore, the nanowire networks are proven to be excellent nanostructures for various electrocatalytic applications.

Based on these two concepts, we fabricated Ag_2S-CoS HNWs with abundant stepped surfaces and defect sites using the Ag_2S seeded growth method. The synthesized Ag_2S-CoS HNWs demonstrated considerably improved OER activity compared to CoS NPs. This enhanced property can be ascribed to the abundant stepped surfaces and defect sites on the surface of the HNWs. The stepped surfaces and defect sites can hold the exposed Co atoms in octahedral sites and are thus considered active sites of cobalt sulfide electrocatalysts. The oxygen binding energies of Ag_2S-CoS HNWs were much stronger than those of CoS. The strong oxygen binding character of Ag_2S-CoS HNWs originates from the exposed active sites due to their hierarchical structure.

2. Experimental section

2.1. Materials

Cobalt nitrate hexahydrate ($Co(NO_3)_2{\cdot}6H_2O$, > 98.0%), Ag nitrate ($AgNO_3$, > 99.0%), sodium diethyldithiocarbamate ($NaS_2CN(C_2H_5)_2$, DDTC > 99.0%), oleylamine ($C_{18}H_{37}N$, > 70.0%), potassium hydroxide (KOH, > 99.9%), ethanol (C_2H_5OH, > 99.8%), n-hexane (C_6H_{14}, > 99.0%) and isopropyl alcohol (C_3H_7OH, > 99.8%) were all purchased from Sigma-Aldrich. Milli-Q ultra-pure water (> 18 MΩ·cm) was used in all experiments.

2.2. Electrocatalyst preparation

Ag_2S-CoS HNWs were prepared by thermal decomposition of the metal ion-DDTC complex Ag_xCo_y-$(S_2CN(C_2H_5)_2)_4$. The precursor powder was prepared by mixing 50 ml of a sodium DDTC aqueous solution (2.50 mmol) with 50 ml of an aqueous solution containing silver nitrate and cobalt nitrate hexahydrate in mole ratios (x:y) of 1:1, 1:4 and 1:8 (total concentration of metal ions = 1.25 mmol), followed by washing with deionized (DI) water several times and drying in a vacuum oven. Fifty milligrams of precursor powder was heat-treated in a tube furnace under a N_2 atmosphere at 180 °C for 30 min. The heat-treated precursor was dissolved in 1 ml of oleylamine in a 25 ml three-neck flask. The solution was degassed thoroughly under vacuum for 1 h to prevent unintended oxidation. Thermal decomposition was conducted at 150 °C for 60 min in a N_2 atmosphere. The resulting suspension was centrifuged, rinsed with a mixed solution of ethanol and n-hexane several times, and dried in a vacuum oven overnight.

2.3. Characterization of Ag_2S-CoS HNWs

The structures of the NWs were analyzed using transmission electron microscopy (TEM, 200 kV Talos F200X, FEI) and energy dispersive X-ray spectroscopy (EDS). The NWs were structurally characterized using a powder X-ray diffractometer (PXRD, SmartLab, Rigaku). Core-level binding energies between Co and S atoms were measured using X-ray photoelectron spectroscopy (XPS, K-alpha, Thermo VG Scientific) with Al Kα radiation (1486.6 eV). All energy data were calibrated to a carbon peak (284.8 eV).

2.4. Electrochemical measurement

Electrocatalysts were tested with a conventional three-electrode configuration with a potentiostat (Interface 1010E, Gamry Instrument). Ag/AgCl (in 4.0 M KCl) and Pt wire were used as reference and counter electrodes, respectively. A glassy carbon rotating disk electrode (RDE, diameter = 5 mm, geometric surface area = 0.196 cm^2) was used as the working electrode. For preparation of catalyst inks, catalysts (5 mg) were dispersed in isopropyl alcohol (0.95 ml) with 5 wt% Nafion (0.05 ml) by sonication for 30 min. The catalyst ink samples (3.5 μl) were dropped onto the glassy carbon electrode and dried under an infrared lamp for 20 min. All electrochemical measurements were conducted in alkaline O_2-saturated 1.0 M KOH media (pH 14). The applied potentials in this work were referenced to a reversible hydrogen electrode (RHE) through standard calibration. The OER was evaluated by measuring linear sweep voltammetry (LSV) over a voltage range of 1.0–1.8 V with a scan rate of 5 mV/s and a rotating speed of 1600 rpm. All of the electrochemical measurements were corrected with iR correction using the CI method implemented in Gamry software. To evaluate the charge transfer resistance, electrochemical impedance spectroscopy (EIS) measurements were carried out by applying an ac voltage of 10 mV in the frequency range of 100–0.1 kHz at 1.53 V (vs. RHE). A chronopotentiometry experiment with 10 mA/cm^2 was carried out for the durability test. LSV was performed before and after the durability test. Double layer capacitance (DLC) was analyzed by cyclic voltammetry (CV) over a voltage range of 8.5–1.05 V with scan rates of 20, 40, 60, 80 and 100 mV/s. DLC was converted to a roughness factor (RF), indicating the relative surface area, referenced to most active electrocatalysts. Specific activity was calculated from the RF-normalized LSV curve at 1.523 V.

2.5. Computational details

For theoretical investigation, GGA-level spin-polarized DFT calculations were performed using a Vienna ab initio simulation (VASP) code with a plane wave basis set. The Perdew − Burke − Ernzerhof (PBE) functional was used to treat electron exchange-correlation terms [21]. The DFT + U method was adopted for the localized Co 3d orbitals with U = 3.52, as reported in previous research [22]. The cut-off energy was 400 eV, and the Brillouin zone was sampled with a 5x5x1 k-point mesh with the Monkhorst-Pack scheme. The convergence criteria were set to 10^{-5} eV and 0.01 eV/Å for electronic and geometrical optimizations, respectively. We constructed (100), (001), (101) and (102) slab models consisting of three layers. The first layer was fixed on the bulk position. The theoretical overpotentials were calculated by a reaction free energy diagram, which is derived from the following equation:

$$\Delta G(U) = \Delta E - \Delta E_{ZPE} - T\Delta S - neU$$

where ΔE is the reaction energy, ΔZPE represents the zero-point energy correction, ΔS is the difference in entropy, and U is the applied potential.

3. Results and discussion

Ag_2S-CoS HNWs with abundant defect sites were synthesized using simple thermal decomposition of the metal ion-DDTC complex. The precursor was prepared by mixing metal precursor and sodium DDTC with targeted compositions (Ag:Co = 1:1, 1:4, 1:8). The thermal decomposition process was conducted at 150 °C for 60 min. At the initial state of the synthesis, the Ag_2S NPs were formed first and can be easily synthesized, even at room temperature. With increasing temperature of the solution, the CoS clusters were gradually generated by the thermal decomposition of the Co-DDTC organometallic complex. This one-step seeded growth has been used to synthesize a variety of binary heterostructures [23,24]. It has been reported that Ag_2S NPs act as universal seeds for the growth of other metal sulfide nanowires, such as ZnS, MnS

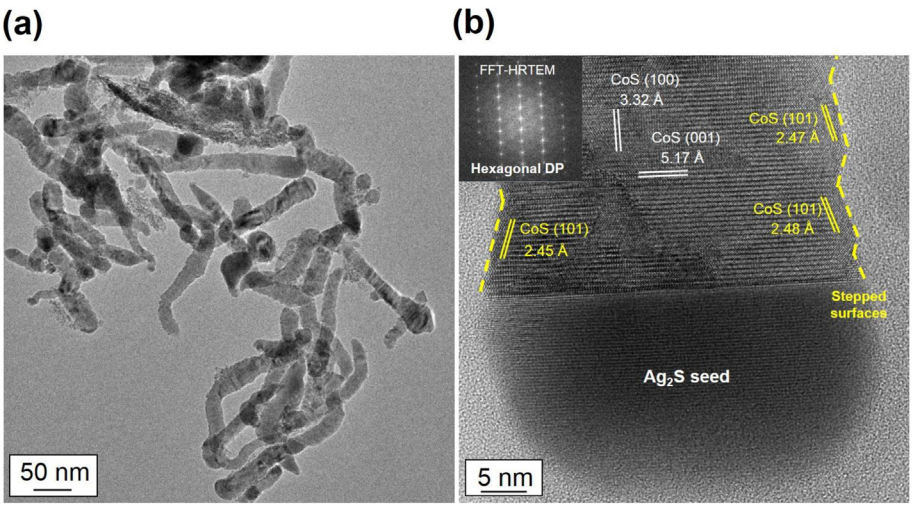

Fig. 1. (a) TEM images, and (b) HRTEM of Ag_2S-CoS_14; inset (b) is its fast Fourier transform (FFT)-selected area electron diffraction (SAED) pattern; yellow dotted lines indicate stepped surfaces. (For interpretation of the references to colour in this figure legend, the reader is referred to the web version of this article.)

and CdS, with many defects [25]. The CoS HNWs were successfully grown on Ag_2S NPs formed at the initial state of synthesis. To the best of our knowledge, chemical synthesis of CoS nanowires has not yet been reported.

The TEM images and size distributions of the synthesized Ag_2S-CoS HNWs with compositions of 1:1, 1:4, and 1:8 are shown in Fig. 1(a) and Fig. S1(a-c). The lengths of Ag_2S-CoS HNWs can be tuned by controlling the ratio of Ag:Co; longer HNWs were formed as the ratio of Co/Ag increased. At a precursor composition ratio > 1:4, the HNWs started to increase in width. The lengths of Ag_2S-CoS_11, Ag_2S-CoS_14, and Ag_2S-CoS_18 were measured to be 87.7 nm, 157.4 nm, and 204.3 nm, respectively. Ag_2S-seeded growth of CoS HNWs is clearly verified by EDS elemental mapping; Ag exists only at the seed, and Co exists only in the body of the HNWs, as shown in Fig. S2. CoS is a hexagonal structure; S atoms have a hexagonal close packed (HCP) structure, and Co atoms are located in the octahedral sites. The octahedral sites of Co atoms are considered active sites of cobalt sulfide electrocatalysts for the OER. Therefore, the CoS phase of the Ag_2S-CoS HNWs is beneficial for designing highly active electrocatalysts. The Ag_2S-CoS HNWs have excellent crystallinity (Fig. 1(b)). The hexagonal structure was confirmed from the fast Fourier transformed diffraction pattern (inset of Fig. 1(b)). Fig. 2 shows the X-ray diffraction (XRD) analysis of the synthesized HNWs, indicating the mixed phase of Ag_2S and CoS. As the Co/Ag ratio was increased, the Ag_2S phase indeed decreased. Zhu et al. have shown that Ag_2S plays an important role in the subsequent growth of hexagonal-phase ZnS [26]. Cubic ZnS NPs were obtained without Ag_2S seeds. Similarly, the CoS nanowires were not synthesized without Ag_2S NP seeds, as shown in Fig. S3. Interestingly, the synthesized CoS NPs (Co_3S_4) possess different crystalline phases of cubic structure than Ag_2S-CoS HNWs (Fig. S4(a-b)). The hexagonal phase of CoS is metastable phase [27], compared to cubic phases such as Co_9S_8, Co_3S_4, and CoS_2. It can be known that Ag_2S NP seeds force the CoS to grow with the metastable phase. Additionally, XPS analysis was conducted to identify chemical bonding states and elemental components of Ag_2S-CoS HNWs (see the Fig. S5(a-d), Table S2). All XPS spectra were calibrated with respect to C 1 s peak (C−C, 284.8 eV). There exists four deconvoluted Co $2p_{3/2}$ peaks, which correspond to Co^{3+} (778.0 eV), Co^{2+} (781.2 eV), and shakeup satellite (~ 783 and ~ 785 eV) peaks, respectively, as shown in Fig. S5(a) [28]. The CoS is a non-stoichiometric compound, showing a mixed oxidation state of Co^{3+} and Co^{2+}. Fig. S5(b) indicates typical S $2p_{3/2}$ and $2p_{1/2}$ spectra of metal sulfide, located in 161.5 eV and 162.7 eV, respectively [29]. Ag $3d_{5/3}$ spectrum corresponds to the Ag_2S (367.9 eV) [30], as shown in Fig. S5(c). This XPS analysis is well agreement with previous hexagonal phase CoS reports [9,15,16]. Furthermore, XPS quantitative analysis was conducted to confirm the surface composition of Ag_2S-CoS HNWs. The XPS compositions were calculated with the area under the spectrum and sensitivity factors of each element [31]. As shown in Table S2, as increasing Co compositions, it can be seen that relative compositions of Ag are decreasing. This is same results with the EDS compositional analysis (see the Table S1).

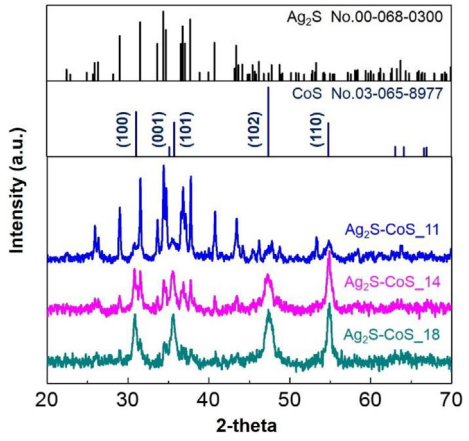

Fig. 2. PXRD analysis of Ag_2S-CoS_11, Ag_2S-CoS_14, and Ag_2S-CoS_18.

The electrochemical activities of the Ag_2S-CoS HNWs toward the OER were investigated by recording LSV over a voltage range of 1.0–1.8 V (vs. RHE). Typically, the applied voltage, showing 10 mA/cm^2 of geometric current density, minus 1.23 V is considered the overpotential for the OER. As shown in Fig. 3(a), Ag_2S-CoS_14 exhibits the best OER performance, with only 275 mV of overpotential. Only 9% increase of overpotential for Ag_2S-CoS_14 was achieved after 2 h of the durability test at a constant current density of 10 mA/cm^2 (Fig. S6(a)). The activity order is Ag_2S-CoS_14 (275 mV) > Ag_2S-CoS_18 (334 mV) > CoS (353 mV) > Ag_2S-CoS_11 (451 mV) > AgS. Fig. 3(b) shows the Tafel plot, generally indicating the reaction kinetics of the electrocatalysts. The Ag_2S-CoS_14 HNWs possess the fastest kinetics and the lowest Tafel slope (77.1 $mVdec^{-1}$; see Fig. 3(b)), while the other electrocatalysts have higher slopes: Ag_2S-CoS_18 = 92.1, CoS = 93.0, and Ag_2S-CoS_11 = 240 $mVdec^{-1}$. The electrical conductivity of the electrocatalysts is directly related to the charge transfer resistance (Fig. S6(b)). Generally, nanowires with higher aspect ratios show better electrical conductivity [32]. As expected, the longest HNW (Ag_2S-CoS_18) showed the lowest charge transfer resistance (only

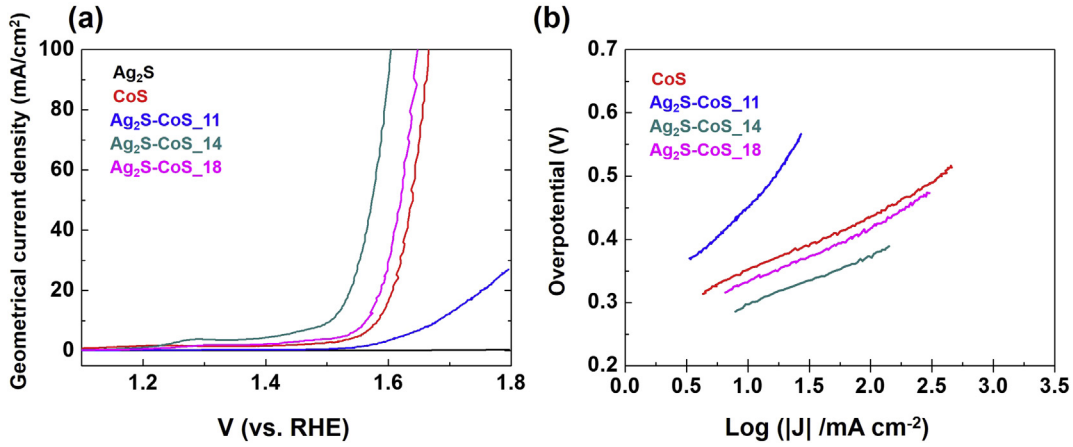

Fig. 3. (a) LSV and (c) Tafel plot for Ag_2S, CoS, Ag_2S-CoS_11, Ag_2S-CoS_14, and Ag_2S-CoS_18; all electrochemical measurements were conducted in O_2-saturated 1.0 M KOH electrolyte.

1.3 Ω). Interestingly, the most active electrocatalyst is Ag_2S-CoS_14, which shows a relatively high resistance (2.5 Ω). Ag_2S, CoS, and Ag_2S-CoS_11 showed resistances of 8700 Ω, 3.2 Ω, and 250 Ω, respectively. To compare the intrinsic properties of electrocatalysts, electrochemical DLCs were measured in the nonfaradic region. The RFs of each electrocatalyst were calculated based on the DLC (Fig. S7 and Table S3). Fig. S8(a) shows RF-normalized LSV curves for the electrocatalysts, which indicate specific activity. RF-normalized current densities at 1.523 V (300 mV of overpotential) are compared in Fig. S8(b). Ag_2S-CoS_14 HNWs exhibit 12-fold higher specific activity than CoS NPs. It can be known that the Ag_2S-CoS_14 HNWs pronounce an excellent OER performance (275 mV), when compared with recently reported CoS works, as shown in Table S4. From the above electrochemical investigation, it should be clarified that the OER performance of Ag_2S-CoS_14 is much better than that of Ag_2S-CoS_18, with better charge transfer resistance. It can be expected that other factors indeed affect OER activity in addition to than electrical conductivity. One possible reason for the lower activity and the higher charge transfer resistance of Ag_2S-CoS_18 is the sulfur-terminated surfaces, which deactivate the exposed octahedral Co sites. As shown in the EDS composition (Table S1) and the XPS quantitative analyses (Table S2), the Ag_2S-CoS_18 HNWs possess much a higher content of sulfur, compared to their stoichiometric composition. Fig. S9 clearly shows the excess amount of sulfur with a ratio of measured composition and their stoichiometric one. In our synthesis of Ag_2S-CoS HNWs, metal-DDTC complex was used as a precursor of metal cations and sulfur anions. The Co-$(DDTC)_2$ precursor contains 2-times of sulfur atoms compared to the Ag-DDTC, because Co has divalance ionic state. Thus, as we increase the Co composition, the amount of sulfur anions will be excessed gradually.

To understand the unique electrochemical properties of Ag_2S-CoS HNWs, we conducted DFT calculations on various slabs of hexagonal-phase CoS. We modeled the (100), (101), (101), and (102) slab surfaces consisting of 16 Co atoms and 16 S atoms. Each of these surfaces have several terminations. We derived the most stable termination of each surface by calculating the surface energies. The modeled (101) and (102) surfaces are shown in Fig. S10(a-b). Based on the modeled slabs, the Gibbs free energy diagrams were calculated for the OER, as shown in Fig. 4(a–b). As expected, the higher-indexed surfaces, such as (101) and (102), have much lower theoretical overpotentials. These better OER properties are due to the higher oxygen binding energies of the surfaces. Xia et al. reported that NiCoSe nanoarrays with stepped surfaces exhibited good OER performance [33]. Additionally, Kibsgaard el al. engineered the surface structure of MoS_2 to preferentially expose edge sites to achieve improved electrocatalysis [34]. In addition to the stepped surfaces, the Ag_2S-CoS HNWs have very abundant defect sites, such as twinning and dislocations at the bent region of HNWs (see Fig. S8(c)). The seeded growth of hexagonal-phase CoS could generate a very high strain at the interface due to the very large difference in lattice spacing between the Ag_2S seed and the hexagonal-phase CoS, which could generate the stepped surfaces and the bent regions possessing abundant defect sites.

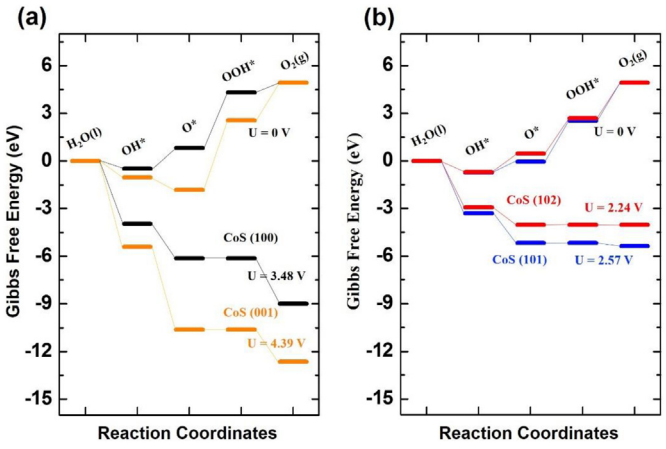

Fig. 4. Gibbs free energy diagram for the OER on (a) low-index surfaces (CoS (100) and (001)) and (b) stepped surfaces (CoS (101) and (102)), respectively.

The high electrochemical activity of Ag_2S-CoS_14 HNWs originates from the fact that the HNWs possess the abundant stepped surfaces and defect sites at every bent region, as shown in Fig. 2(a) and Fig. S8(c). Fig. S8(d) shows a schematic diagram of the suggested reason for the improved OER activity of Ag_2S-CoS HNWs. The exposed octahedral Co sites are well known as active sites for the OER [35]. The active sites can be generated by creating more stepped surfaces, defect sites or disordered structures [33]. Higher oxygen binding energy at the stepped surfaces can promote water adsorption and water oxidation. Moreover, the networks of Ag_2S-CoS HNWs have shown superior electrical conductivity and charge transfer characteristics. These two factors possibly improved the OER activity of the Ag_2S-CoS HNWs. This research will shed light on the future design of bifunctional electrocatalysts such as metal sulfide, phosphide, and selenide.

4. Conclusion

In this work, Ag_2S-CoS HNWs with abundant stepped surfaces and defect sites were successfully synthesized by simple thermal decomposition of organometallic complexes, in conjunction with the Ag_2S seeded growth method. Ag_2S-CoS showed a hexagonal crystalline phase for CoS, which was not detected in the conventional thermal

decomposition method. The hexagonal phase of CoS consists of S atoms in an HCP site and Co atoms in an octahedral site. The abundant octahedral sites of the CoS phase can be beneficial to OER activity. Ag_2S-CoS_14 HNWs showed the best OER performance: an overpotential of 275 mV, a Tafel slope of 77.1 $mVdec^{-1}$, and charge transfer resistance of 2.5 Ω. The improved OER activity was observed for over 2 h. The abundant stepped surfaces and defect sites generated exposed octahedral sites at the surface, which served as active sites with high oxygen binding energy. Additionally, HNW networks showed superior charge transfer characteristics due to their electrical junctions between HNWs. The structural features of Ag_2S-CoS HNWs promoted OER activity considerably.

Acknowledgments

This research was supported by a National Research Foundation (NRF) of Korea grant funded by the Korean Government (No. NRF-2015R1A5A1037627). This research was supported by the Creative Materials Discovery Program through the NRF of Korea funded by the Ministry of Science, ICT and Future Planning (NRF-2016M3D1A1900035).

Appendix A. Supplementary data

Supplementary data to this article can be found online at https://doi.org/10.1016/j.catcom.2019.105749.

References

[1] B. Sorensen, A.H. Petersen, C. Juhl, H. Ravn, C. Sondergren, P. Simonsen, K. Jorgensen, L.H. Nielsen, H.V. Larsen, P.E. Morthorst, L. Schleisner, F. Sorensen, T.E. Pedersen, Hydrogen as an energy carrier: scenarios for future use of hydrogen in the Danish energy system, Int. J. Hydrogen Energ. 29 (1) (2004) 23–32.

[2] M.R. Rahimpour, Enhancement of hydrogen production in a novel fluidized-bed membrane reactor for naphtha reforming, Int. J. Hydrogen Energ. 34 (5) (2009) 2235–2251.

[3] W.Y. Tong, A. West, K. Cheung, K.M. Yu, S.C.E. Tsang, Dramatic effects of gallium promotion on methanol steam reforming cu-ZnO catalyst for hydrogen production: formation of 5 angstrom copper clusters from Cu-$ZnGaO_x$, ACS Catal. 3 (6) (2013) 1231–1244.

[4] T.R. Cook, D.K. Dogutan, S.Y. Reece, Y. Surendranath, T.S. Teets, D.G. Nocera, Solar energy supply and storage for the legacy and non legacy worlds, Chem. Rev. 110 (11) (2010) 6474–6502.

[5] J.W. Huang, Y.H. Sun, X.C. Du, Y.D. Zhang, C.Y. Wu, C.Y. Yan, Y.C. Yan, G.F. Zou, W.Q. Wu, R.F. Lu, Y.R. Li, J. Xiong, Cytomembrane-structure-inspired active Ni-N-O Interface for enhanced oxygen evolution reaction, Adv. Mater. 30 (39) (2018).

[6] W.T. Hong, M. Risch, K.A. Stoerzinger, A. Grimaud, J. Suntivich, Y. Shao-Horn, Toward the rational design of non-precious transition metal oxides for oxygen electrocatalysis, Energy Environ. Sci. 8 (5) (2015) 1404–1427.

[7] J.H. Han, M. Kwak, Y. Kim, J. Cheon, Recent advances in the solution-based preparation of two-dimensional layered transition metal chalcogenide nanostructures, Chem. Rev. 118 (13) (2018) 6151–6188.

[8] J.W. Huang, Y.H. Sun, Y.D. Zhang, G.F. Zou, C.Y. Yan, S. Cong, T.Y. Lei, X. Dai, J. Guo, R.F. Lu, Y.R. Li, J. Xiong, A new member of electrocatalysts based on nickel metaphosphate nanocrystals for efficient water oxidation, Adv. Mater. 30 (5) (2018).

[9] K. Prabakaran, M. Lokanathan, B. Kakade, Three dimensional flower like cobalt sulfide (CoS)/functionalized MWCNT composite catalyst for efficient oxygen evolution reactions, Appl. Surf. Sci. 466 (2019) 830–836.

[10] Z.F. Huang, J.J. Song, K. Li, M. Tahir, Y.T. Wang, L. Pan, L. Wang, X.W. Zhang, J.J. Zou, Hollow cobalt-based bimetallic sulfide polyhedra for efficient all-pH-value electrochemical and photocatalytic hydrogen evolution, J. Am. Chem. Soc. 138 (4) (2016) 1359–1365.

[11] Y.D. Niu, X. Qian, J. Zhang, W.M. Wu, H.Y. Liu, C. Xu, L.X. Hou, Stepwise synthesis of CoS_2-C@CoS_2 yolk-shell nanocages with much enhanced electrocatalytic performances both in solar cells and hydrogen evolution reactions, J. Mater. Chem. A 6 (25) (2018) 12056–12065.

[12] H.J. Xu, J. Cao, C.F. Shan, B.K. Wang, P.X. Xi, W.S. Liu, Y. Tang, MOF-derived hollow CoS decorated with CeO_x nanoparticles for boosting oxygen evolution reaction electrocatalysis, Angew. Chem. Int. Edit. 57 (28) (2018) 8654–8658.

[13] N.T. Suen, S.F. Hung, Q. Quan, N. Zhang, Y.J. Xu, H.M. Chen, Electrocatalysis for the oxygen evolution reaction: recent development and future perspectives, Chem. Soc. Rev. 46 (2) (2017) 337–365.

[14] X.Y. Ma, W. Zhang, Y.D. Deng, C. Zhong, W.B. Hu, X.P. Han, Phase and composition controlled synthesis of cobalt sulfide hollow nanospheres for electrocatalytic water splitting, Nanoscale 10 (10) (2018) 4816–4824.

[15] P. Guo, Y.X. Wu, W.M. Lau, H. Liu, L.M. Liu, CoS nanosheet arrays grown on nickel foam as an excellent OER catalyst, J. Alloy Compd. 723 (2017) 772–778.

[16] Z.F. Dai, H.B. Geng, J. Wang, Y.B. Luo, B. Li, Y. Zong, J. Yang, Y.Y. Guo, Y. Zheng, X. Wang, Q.Y. Yan, Hexagonal-phase cobalt monophosphosulfide for highly efficient overall water splitting, ACS Nano 11 (11) (2017) 11031–11040.

[17] C. Zhang, S.J. Liu, Z.Z. Mao, X. Liang, B.H. Chen, Ag-Ni core-shell nanowires with superior electrocatalytic activity for alkaline hydrogen evolution reaction, J. Mater. Chem. A 5 (32) (2017) 16646–16652.

[18] H.W. Huang, K. Li, Z. Chen, L.H. Luo, Y.Q. Gu, D.Y. Zhang, C. Ma, R. Si, J.L. Yang, Z.M. Peng, J. Zeng, Achieving remarkable activity and durability toward oxygen reduction reaction based on ultrathin Rh-doped Pt nanowires, J. Am. Chem. Soc. 139 (24) (2017) 8152–8159.

[19] M.F. Li, Z.P. Zhao, T. Cheng, A. Fortunelli, C.Y. Chen, R. Yu, Q.H. Zhang, L. Gu, B.V. Merinov, Z.Y. Lin, E.B. Zhu, T. Yu, Q.Y. Jia, J.H. Guo, L. Zhang, W.A. Goddard, Y. Huang, X.F. Duan, Ultrafine jagged platinum nanowires enable ultrahigh mass activity for the oxygen reduction reaction, Science 354 (6318) (2016) 1414–1419.

[20] H. Xu, J.J. Wei, M. Zhang, J. Wang, Y. Shiraishi, L. Tian, Y. Du, Self-supported nickel-cobalt nanowires as highly efficient and stable electrocatalysts for overall water splitting, Nanoscale 10 (39) (2018) 18767–18773.

[21] J.P. Perdew, K. Burke, M. Ernzerhof, Generalized gradient approximation made simple, Phys. Rev. Lett. 77 (18) (1996) 3865–3868.

[22] M. Bajdich, M. Garcia-Mota, A. Vojvodic, J.K. Norskov, A.T. Bell, Theoretical investigation of the activity of cobalt oxides for the electrochemical oxidation of water, J. Am. Chem. Soc. 135 (36) (2013) 13521–13530.

[23] C. Lee, K. Shin, Y.J. Lee, C. Jung, H.M. Lee, Effects of shell thickness on Ag-Cu_2O core-shell nanoparticles with bumpy structures for enhancing photocatalytic activity and stability, Catal. Today 303 (2018) 313–319.

[24] A. Sarvi, G.A. Gelves, U. Sundararaj, Facile one step-synthesis and characterisation of high aspect ratio core-shell copper-polyaniline nanowires, Can. J. Chem. Eng. 92 (7) (2014) 1207–1212.

[25] S.T. Chen, S. Thota, G. Reggiano, J. Zhao, Generalized seeded growth of Ag-based metal chalcogenide nanorods via controlled chalcogenization of the seeds, J. Mater. Chem. C 3 (45) (2015) 11842–11849.

[26] G.X. Zhu, Z. Xu, Controllable growth of semiconductor heterostructures mediated by bifunctional Ag_2S nanocrystals as catalyst or source-host, J. Am. Chem. Soc. 133 (1) (2011) 148–157.

[27] A.E. Powell, J.M. Hodges, R.E. Schaak, Preserving both anion and cation sublattice features during a nanocrystal cation-exchange reaction: synthesis of metastable wurtzite-type CoS and MnS, J. Am. Chem. Soc. 138 (2) (2016) 471–474.

[28] M.C. Biesinger, B.P. Payne, A.P. Grosvenor, L.W.M. Lau, A.R. Gerson, R.S. Smart, Resolving surface chemical states in XPS analysis of first row transition metals, oxides and hydroxides: Cr, Mn, Fe, Co and Ni, Appl. Surf. Sci. 257 (7) (2011) 2717–2730.

[29] S.W. Goh, A.N. Buckley, B. Gong, R. Woods, R.N. Lamb, L.J. Fan, Y.W. Yang, Thiolate layers on metal sulfides characterised by XPS, ToF-SIMS and NEXAFS spectroscopy, Miner. Eng. 21 (12–14) (2008) 1026–1037.

[30] C.M. Cova, A. Zuliani, A.R.P. Santiago, A. Caballero, M.J. Munoz-Batista, R. Luque, Microwave-assisted preparation of Ag/Ag_2S carbon hybrid structures from pig bristles as efficient HER catalysts, J. Mater. Chem. A 6 (43) (2018) 21516–21523.

[31] C. Lee, N.R. Kim, J. Koo, Y.J. Lee, H.M. Lee, Cu-Ag core-shell nanoparticles with enhanced oxidation stability for printed electronics, Nanotechnology 26 (45) (2015).

[32] C.H. Liu, X. Yu, Silver nanowire-based transparent, flexible, and conductive thin film, Nanoscale Res. Lett. 6 (2011).

[33] C. Xia, Q. Jiang, C. Zhao, M.N. Hedhili, H.N. Alshareef, Selenide-based electrocatalysts and scaffolds for water oxidation applications, Adv. Mater. 28 (1) (2016) 77.

[34] J. Kibsgaard, Z.B. Chen, B.N. Reinecke, T.F. Jaramillo, Engineering the surface structure of MoS_2 to preferentially expose active edge sites for electrocatalysis, Nat. Mater. 11 (11) (2012) 963–969.

[35] A. Sivanantham, P. Ganesan, S. Shanmugam, Hierarchical $NiCo_2S_4$ nanowire arrays supported on Ni foam: an efficient and durable bifunctional electrocatalyst for oxygen and hydrogen evolution reactions, Adv. Funct. Mater. 26 (26) (2016) 4661–4672.